CrystEngComm

Synthesis and applications of Porphyrin-based MOFs in removal of pesticide from wastewater: Molecular simulations and experimental studies

Journal:	*CrystEngComm*
Manuscript ID	CE-ART-10-2023-001058.R1
Article Type:	Paper
Date Submitted by the Author:	06-Nov-2023
Complete List of Authors:	Ayman.FM, Fatma; Beni Suef University Taha, Mohamed; Beni Suef University Farghali, Ahmed; Beni Suef University Abdelhameed, Reda; University of Aveiro, Chemistry, CICECO, QOPNA

Synthesis and applications of Porphyrin-based MOFs in removal of pesticide from wastewater: Molecular simulations and experimental studies

Fatma Ayman.FM[a], Mohamed Taha[a], Ahmed A. Farghali[a], Reda M. Abdelhameed[b*]

[a] Materials Science and Nanotechnology Department, Faculty of Postgraduate Studies for Advanced Sciences (PSAS), Beni-Suef University, Beni-Suef, 62511, Egypt.

[b]Applied Organic Chemistry Department, Chemical Industries Research Institute, National Research Centre, 33 EL Buhouth St., Dokki, Giza 12622, Egypt.

*Corresponding author (Reda M. Abdelhameed, E-mail reda_nrc@yahoo.com)

Abstract

The high toxicity of pesticides to the ecosystem and humans has made their removal from water urgent. However, the properties of the insecticide made it challenging to complete the removal process with high adsorption capacity and exceptional selectivity. Biocompatible porphyrin-based MOFs with good adsorption capacity make them the best choice for removing methomyl pesticides from wastewater due to their large surface area and high porosity. In this work, iron- porphyrin-based MOFs (Fe-TCPP), zinc-porphyrin-based MOFs (Zn-TCPP) and copper-porphyrin-based MOFs (Cu-TCPP) were synthesized and investigated to remove methomyl from water. Besides the characterizations of porphyrin-based MOFs with PXRD, FTIR, and FESEM, Langmuir and Freundlich isotherm models were used to describe adsorption behavior. Fe-TCPP showed higher adsorption capacity (Q_m) than Zn-TCPP and Cu-TCPP, Qm values for Fe-TCPP, Zn-TCPP and Cu-TCPP equal 270.07 mg g^{-1}, 190.97 mg g^{-1}, and 175.95 mg g^{-1}, respectively. Monte Carlo and molecular dynamic simulations were used to study the adsorption mechanism. The computational investigation indicates that the methomyl molecules are aggregated inside the MOF cavities and form hydrogen bond between methomyl pesticide and MOFs structure.

Keywords: Porphyrin, methomyl, adsorption, computational, mechanism

1. Introduction

Metal-organic frameworks (MOFs) which also called porous coordination polymers (PCPs) are promising crystalline materials. MOFs have increased in recent years and this due to unrivaled advantages like a large surface area, high porosity and these pores are tunable, all of these characteristics contributed to the use of MOFs in a variety of applications and fields. MOFs were used as heterogenies catalyst, a biological material, luminescent materials, gas storage & separation, food safety, transportable fuel, solar cells, electronic devices, drug release and biosensing and use in adsorption for water treatment [1-11].

One of the most stable MOFs is porphyrin-based MOFs. Porphyrins are stable, hydrophobic compounds that, when combined with high valence metals, can be utilized to make several chemically stable frameworks[12]. Porphyrin-linkers have attracted particular attention because of their distinctive shape and adaptable functionality for a number of applications [3]. Porphyrins are great candidates to serve as building blocks for MOFs due to their stiffness and robust structures. In recent years, porphyrin-based MOFs have been used in a variety of applications, it was used in biomedical application such as cancer treatment, photodynamic and radiation therapy [13]. Also, it was used as sensor and photocatalytic materials which used as electrochemical sensor to detect DNA [14]. Porphyrin-based MOFs acted as a photocatalyst to reduce CO_2 to CH_4 in the presence of UV/visible radiation [15]. Moreover, porphyrin-based MOFs were used in water treatment applications to remove methyl orange and methyl blue dyes[16], antibiotics oxytetracycline and tetracycline hydrochloride [17] from wastewater.

Water treatment has become an important matter, especially with the increase in water pollution which threatens the human live and environment[18]. Pesticides are one of the most pollutants that accumulate in water and soil and cause a lot of harm to humans and the ecosystem[19, 20]. In addition, pesticides are relatively stable in soil and water[21]. Methomyl (S-methyl-N-(methylcarbamoyloxy)-thioacetimide) (MET) is an oxime insecticide

of the carbamate family; it is frequently used to suppress the eggs, larvae, and adults of many pests[22]. WHO (World Health Organisation), EPA (Environmental Protection Agency, USA), and EC (European Commission) have all categorized it as an extremely toxic and harmful pesticide[22, 23].

Removal of environmental pollutants is becoming more critical due to their direct impact on human resources [24-27]. There are several methods applied to remove and degrade methomyl from water such ultrasonic and hydrodynamic cavitation, oxidation, photo-Fenton process and adsorption[23]. The adsorption technique is inexpensive, rapid and reproducible technique and it can remove contaminants from the aqueous media efficiently. MOFs were used to remove pesticide from polluted water by adsorption technique. ZIF-8@Lignin was used to remove methomyl from wastewater, ZIF-8@Lignin has an adsorption capacity of 324.6 mg/g[28]. UiO-67/GO has been used as an adsorbent to remove glyphosate from contaminated water, UiO-67/GO has adsorption capacity about 482.69 mg/g[29]. Ethion and prothiofos removed from polluted water by ZIF-8 and ZIF-67 which the uptake of prothiophos (366.7 and 261.1 mg/g) is greater than that of ethion (279.3 and 210.8 mg/g, respectively)[30]. Cu-BTC@Cotton composite also used to remove ethion organophosphorus pesticide and adsorption capacity rich 182 mg\g[31]. MOF@Ox-cotton hybrids used to remove pesticide from wastewater, it was removed diazinon and chlorpyrifos pesticide and adsorption capacity rich to 296.77 and 464.69 mg/g, respectively[32].

In this work we prepared porphyrin based MOFs (Fe-TCPP, Zn-TCPP and Cu-TCPP) to selective removal of methomyl pesticide from wastewater. Fe-TCPP, Zn-TCPP and Cu-TCPP were synthesized and characterized by scanning electron microscopy (SEM), X-ray diffraction (XRD) and Fourier transform infrared spectroscopy (FTIR). The isotherms and kinetics modeling was applied to test the behavouir of methomyl adsorption onto Fe-TCPP, Zn-TCPP and Cu-TCPP. The mechanism of methomyl adsorption onto porphyrin based MOFs were also studied using computational modeling.

2. Experimental section

2.1. Materials

4-Formylbenzoic acid (97 % Sigma–Aldrich), Pyrrole and propionic acid 99.9 % (purchased from ADVENT). N,N-dimethylformamide (DMF), methanol 99.8% (Fisher chemical), Copper nitrate trihydrate ($Cu(NO_3)_2 \cdot 3H_2O$, 99.9 % Sigma–Aldrich), ferric nitrate hexahydrate ($Fe(NO_3)_2.6H_2O$, 98 % Sigma–Aldrich), zinc nitrate hexahydrate ($Zn(NO_3)_2 \cdot 6H_2O$, 99 % Sigma–Aldrich).

2.2 Synthesize of Cu-TCPP, Zn-TCCP and Fe-TCPP

The linker 4,4′,4″,4‴-(5,10,15,20-porphyrintetrayl)- tetra benzoic acid (H_6TCPP) was synthesized using methods described in the literature[33-35]. Fe-TCPP was synthesized as follow: 1.212 g of ($Fe(NO_3)_2(H_2O)_6$) and 0.790 g of ligand H_6TCPP dissolved in mixture of (30 ml DMF & 5 ml methanol) (v:v 3:1), then put in flask and heated at 80 ^{0}C for then crystal were washed three times with methanol and collected by centrifuging at 8000 r.p.m for 10 min finally the obtain bulk 3D FeTCPP MOF were dispersed in methanol ,then we filtered it and leave it to dry. Zn-TCPP was synthesized as previous one with some modification as follow: 0.891 g of $Zn(NO_3)_2 \cdot 6H_2O$ and 0.790 g of ligand H_6TCPP dissolved in mixture of (30 ml DMF & 5 ml methanol) (v:v 3:1) , then put in flask and heated at 80 ^{0}C for then crystal were washed three times with methanol and collected by centrifuging at 8000 r.p.m for 10 min finally the obtain bulk 3D Zn-TCPP MOFs were dispersed in methanol, then we filtered it and leave it to dry. Finally, Cu-TCPP was synthesized as follow: 0.723 of (Cu(NO3)2) and 0.790 g of ligand H_6TCPP dissolved in mixture of (30 ml DMF & 5 ml methanol) (v:v 3:1) , then put in flask and heated at 80 ^{0}C for then crystal were washed three times with methanol and collected by centrifuging at 8000 r.p.m for 10 min finally the obtain bulk 3D Cu-TCPP MOF were dispersed in methanol, then we filtered it and leave it to dry.

2.3. Characterization

Several methods were used to characterize the structure and morphology of Cu-TCPP, Zn-TCPP and Fe-TCPP. With a wavenumber range of 4000-400, FTIR spectroscopy was carried out using a JASCO FT-IR-4100 instrument (Tokyo, Japan). Cu K monochromatic radiation with a high intensity (λ = 1.5418) was subjected to powder X-ray diffraction (PRXD, Philips X'Pert MPD diffractometer). The sample was scanned at a rate of 8 (°/min) throughout a range of 2 = 5 to 80° at room temperature. Cu-TCPP, Zn-TCPP and Fe-TCPP surface area, pore volume, and pore volume were measured using Micromeritics ASAP2020 (Norcross, Georgia) and Brunauer-Emmett-Teller (BET) analysis of nitrogen adsorption and desorption isotherms at 77.35 K. Scanning electron microscopy was used to study the microstructure and form of beads (SEM- Hitachi-S4800, Tokyo, Japan). The changing amount of methomyl absorbed on of Cu-TCPP, Zn-TCPP and Fe-TCPP were monitored using a UV-1650 (Shimadzu, Tokyo, Japan) spectrophotometer (200-800 nm).

2.4. Adsorption experiments

The following batch approach was used to fix the optimized time of the adsorption: for each experiment, 30 mg of Cu-TCPP, Zn-TCPP and Fe-TCPP were combined with 100 mL of methomyl (100 mg L^{-1}). The study was done on the impact of contact time over various time periods (5-180 minutes) at room temperature. To determine the isotherm of adsorption, defined concentration of methomyl in an airtight vial was combined with 30 mg of Cu-TCPP, Zn-TCPP and Fe-TCPP. The solution is then stirred at room temperature for 180 minutes. Following the adsorption procedure, the adsorbent was separated by filtering, and the residual concentration was assessed using Shimadzu UV-visible spectroscopy with 1 cm quartz cells at 275 nm. The equation shown below was used to compute the percentage of methomyl elimination by MOF adsorbents (R (%)):

$$R(\%) = ((C_i - C_e)/C_i) * 100 \quad (1)$$

where C_e (mg L^{-1}) denotes the solution's ultimate concentration following methomyl adsorption and C_i (mg L^{-1}) denotes the solution's starting concentration prior to adsorption. The following equation was used to determine the equilibrium absorption capacity (Q_e) of carbaryl[36, 37]:

$$Q_e = (C_i - C_e)V/m \quad (2)$$

where m is the mass of the adsorbent (g), C_i and C_e are the methomyl starting and equilibrium concentrations (mg L^{-1}), respectively; and V is the volume of the solution.

2.5. Computational studies

The Fe-TCPP, Zn-TCPP, and Cu-TCPP MOFs were constructed from Ga-TCPP taken from Rhauderwiek et al.[38], by replacing the gallium atoms with zinc, iron, and copper, respectively. The Forcite, Adsorption Locator, and Sorption modules in Materials Software 2020[39] were used. The optimization of the constructed MOFs and methomyl was performed by the Forcite module. The Universal forcefield[40] was assigned and the convergence tolerance of the optimizations was set as follows: energy = 2.0×10^{-5} Kcal\mol, force = 0.001 Kcal\mol\Å, stress = 0.001 GPa, and displacement = 1.0×10^{-5}Å. The Ewald method and the atom-based summation method were used to treat the electrostatic and van der Waals forces, respectively. The charges were calculated by the QEq method[41]. As an example, figure 1 shows the optimized structure of Fe-TCPP. There are two possible adsorption sites for methomyl molecule, a large opening channel (L) and a small channel (S) between the stacked porphyrin rings (Figure 1).

Monte Carlo (MC) simulations were carried out using the Adsorption Locator and Sorption modules. The Adsorption Locator was applied to find the lowest-energy structures of methomyl adsorbed into the MOF structure. A simulated annealing method was used. The number of cycles was 5 and the steps per cycle were 5×10^4. The maximum and final temperatures were 1.0×10^5 K and 100 K, respectively. The Sorption module was used to

obtain the methomyl/water loading per unit cell by using the Metropolis MC method at a fixed pressure (101.33 kPa) and temperature (298 K). The equilibration and production steps were 1×10^5 and 1×10^6, respectively. The Universal forcefield and the summation method of the optimization process were also used in the Monte Carlo (MC) simulations, as well as the molecular dynamics (MD) simulation.

The Forcite module was also used in the MD simulation. The sorbed methomyl and water structures into the MOFs at fixed pressure and temperature were used as input files for the MD simulation. These structures were simulated with NVT ensemble at 298.0 K, 1000 ps total simulation time, and 1 fs time step. The Nose thermostat was used for controlling the temperature.

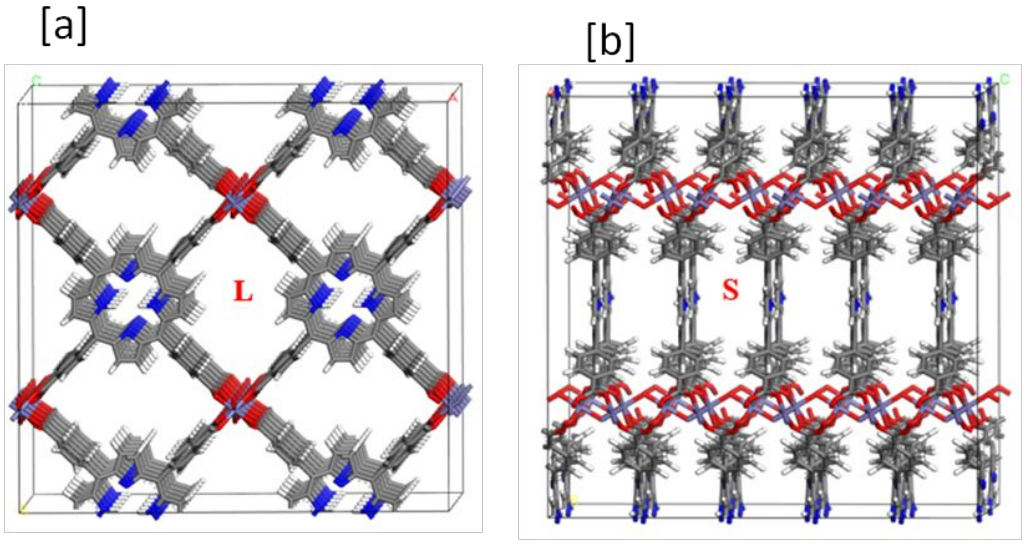

Figure 1. As an example, Fe-TCPP shows a large (L) opening channel and a small (S) channel between the stacked porphyrin rings.

3. Results and Discussion

3.1. Characterization of Cu-TCPP, Zn-TCPP and Fe-TCPP

XRD was used to characterize the crystal structure of the Cu-TCPP, Zn-TCPP and Fe-TCPP MOFs. As illustrated in figure 2, the Cu-TCPP MOFs give typical peaks at 7.51, 9.11, 12.21, 18.12 and 31.2, which ascribes to the tetragonal structure of the Cu-TCPP MOFs. For the Zn-TCPP and Fe-TCPP, most of the crystal diffraction peaks can be detected, and only a peak at

18° corresponding to the (0 0 4) plane is less intensity than Cu-TCPP MOFs. The XRD pattern demonstrates that highly crystalline Cu-TCPP, Zn-TCPP and Fe-TCPP MOFs have been synthesized.

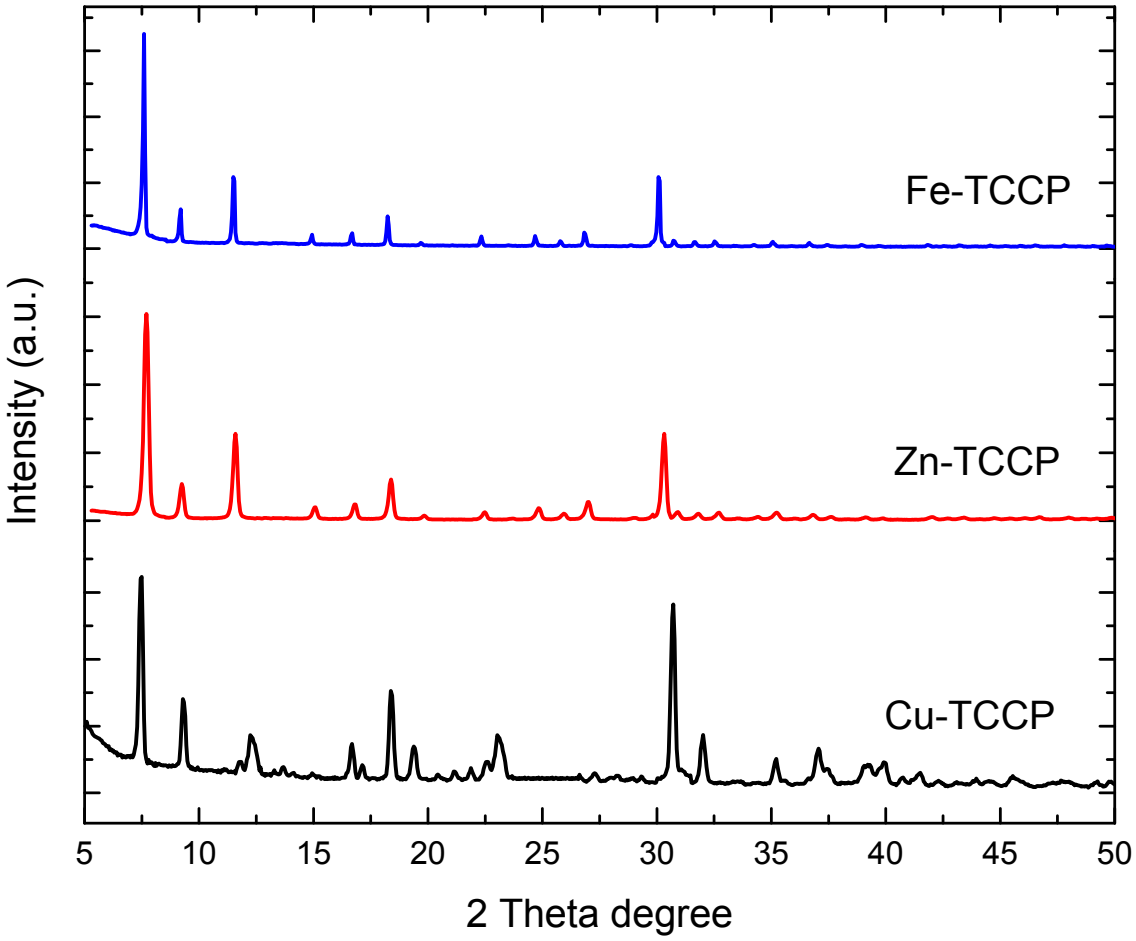

Figure 2. PXRD of Cu-TCPP, Zn-TCPP and Fe-TCPP MOFs

The FTIR spectra of H_2TCPP, Cu-TCPP, Zn-TCPP and Fe-TCPP MOFs were measured to reveal the coordination mode between the metal ions and carboxyl groups of H_2TCPP. As shown in figure 3, H_2TCPP has a distinct peak at 1700 cm^{-1}, attribute to the C = O stretching band. In the spectrum of Cu-TCPP, two dominant peaks located at around 1618 and 1401 cm^{-1} can be assigned to the OC-O-Cu bond. These results indicate that the linker has been successfully metalized by Cu^{2+}, and Cu-TCPP MOFs have been obtained. The FT-IR spectra (Figure 3) proves that Zn-TCPP has two significant peaks of O=C-O-Zn near 1400 and 1615 cm^{-1}, which indicating the formation of a coordination bond between COOH and

Zn^{2+} in TCPP during the synthesis. FT-IR spectra of prepared Fe-TCPP, as shown in Fig. 3, showed absorption peaks around 1600 cm^{-1} and 1400 cm^{-1}, which could be assigned to the C=O asymmetric stretching vibration ($\nu_{asym}C=O$) and the C=O symmetric stretching vibration ($\nu_{sym}C=O$), respectively. The above results indicated the formation of coordination bonds between Fe-based secondary building units and carboxyl groups of the H_2TCPP ligands.

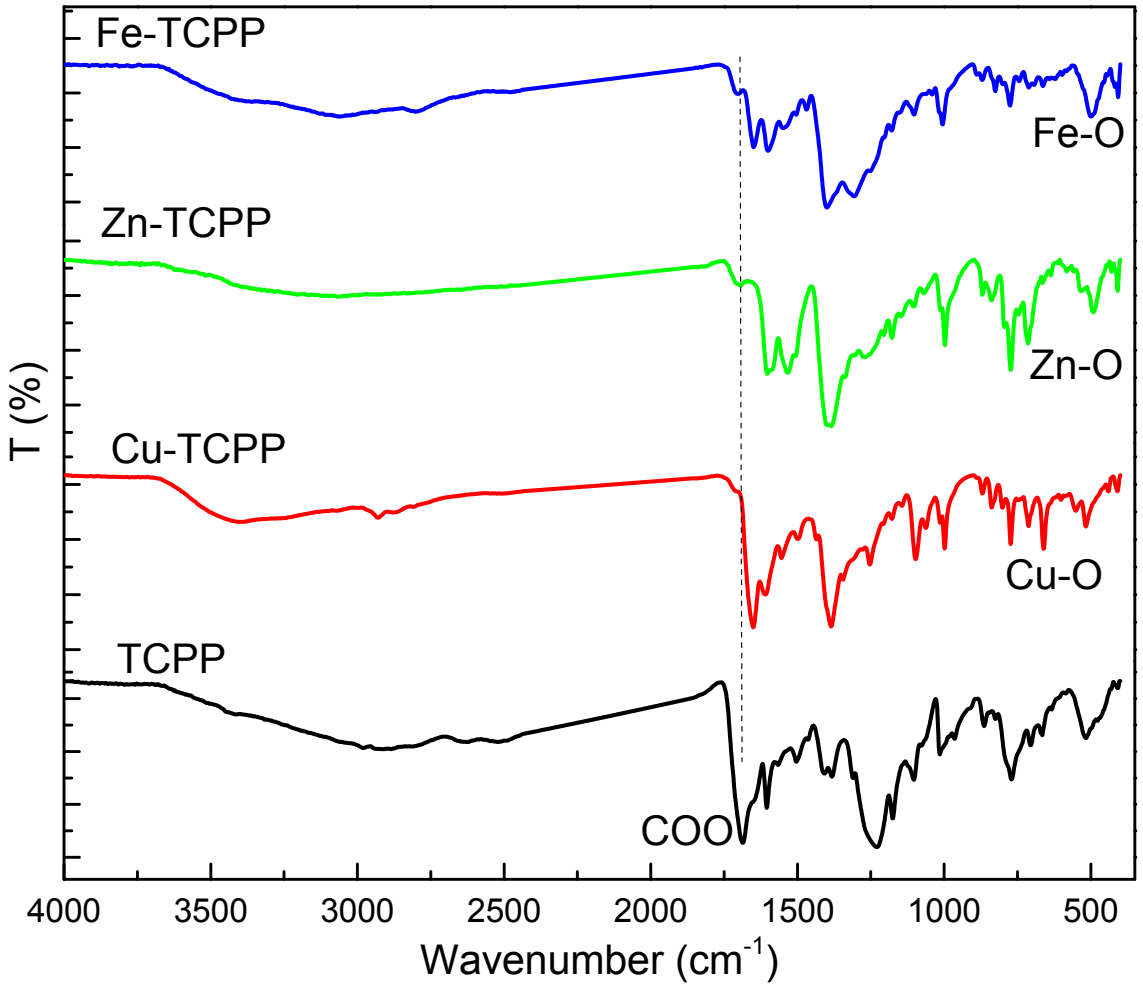

Figure 3. FTIR of Cu-TCPP, Zn-TCPP and Fe-TCPP MOFs

SEM images show that Cu-TCPP presents a lamellar morphology with a size ranging from a few hundred nanometers to a few microns (Figure 4). From the EDS diagram (Figure 4), it can be seen that the C, N, O, and Cu elements in the Cu-TCPP are evenly distributed, and the content of each element is consistent with the element ratio of Cu-TCPP.

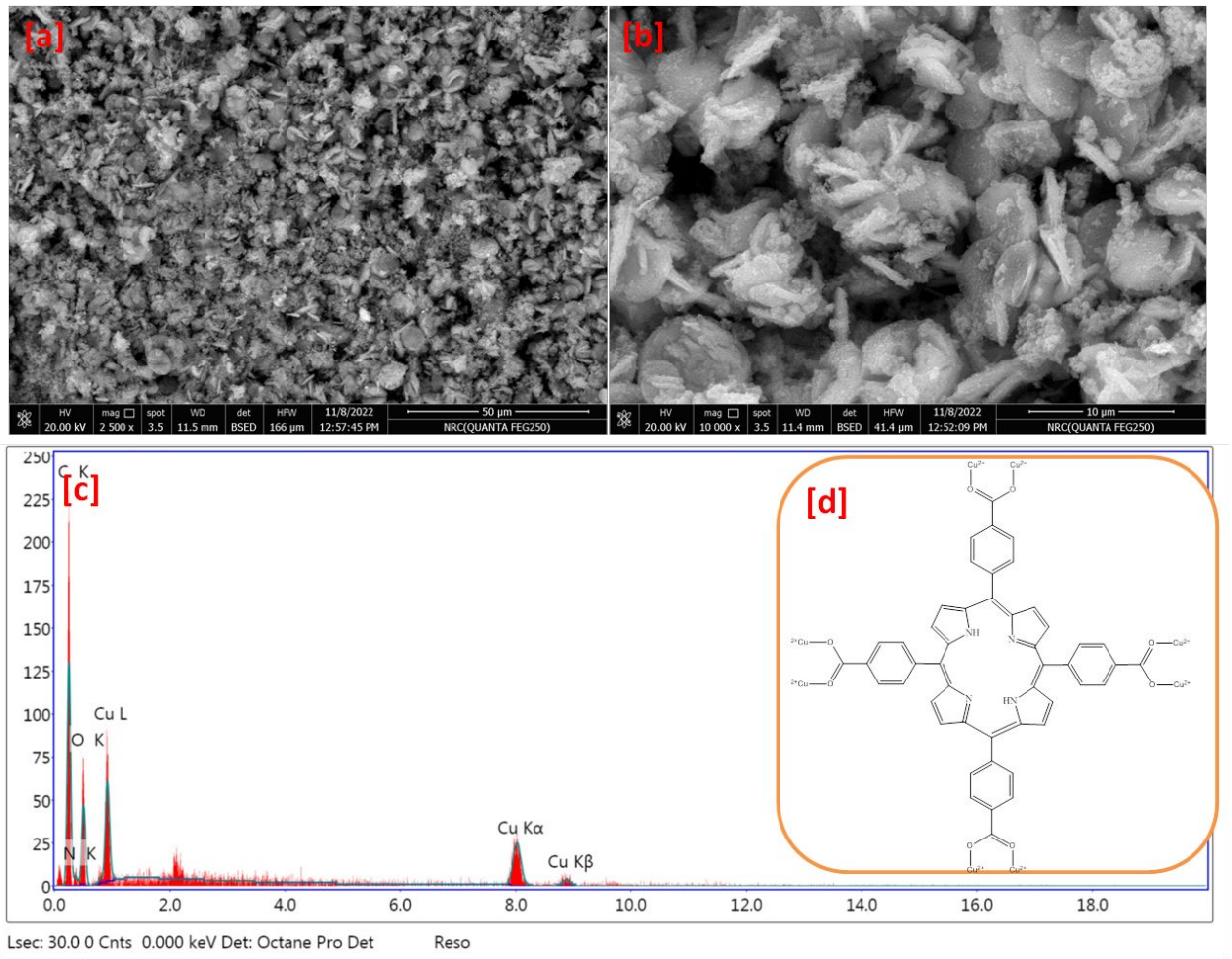

Figure 4. Micrographs and EDX analysis for the synthesized Cu-TCPP

The morphologies of the Zn-TCPP were characterized by SEM. The Zn-TCPP MOFs present a closely spherical structure (Figure 5). The solvothermal method was used in this work to synthesize spherical Zn-TCPP MOF. Scanning electron microscope was used to characterize the microscopic appearance of Zn-TCPP MOF, and proved the successful preparation. Figure 5 displayed that Zn-TCPP MOF is a spherical structure with the order of 400 nm. Furthermore, the prepared Zn-TCPP MOF contained and homogeneously distributed elements of C, N, O, and Zn, which was demonstrated that Zn-TCPP MOF was synthesized successfully (Figure 5).

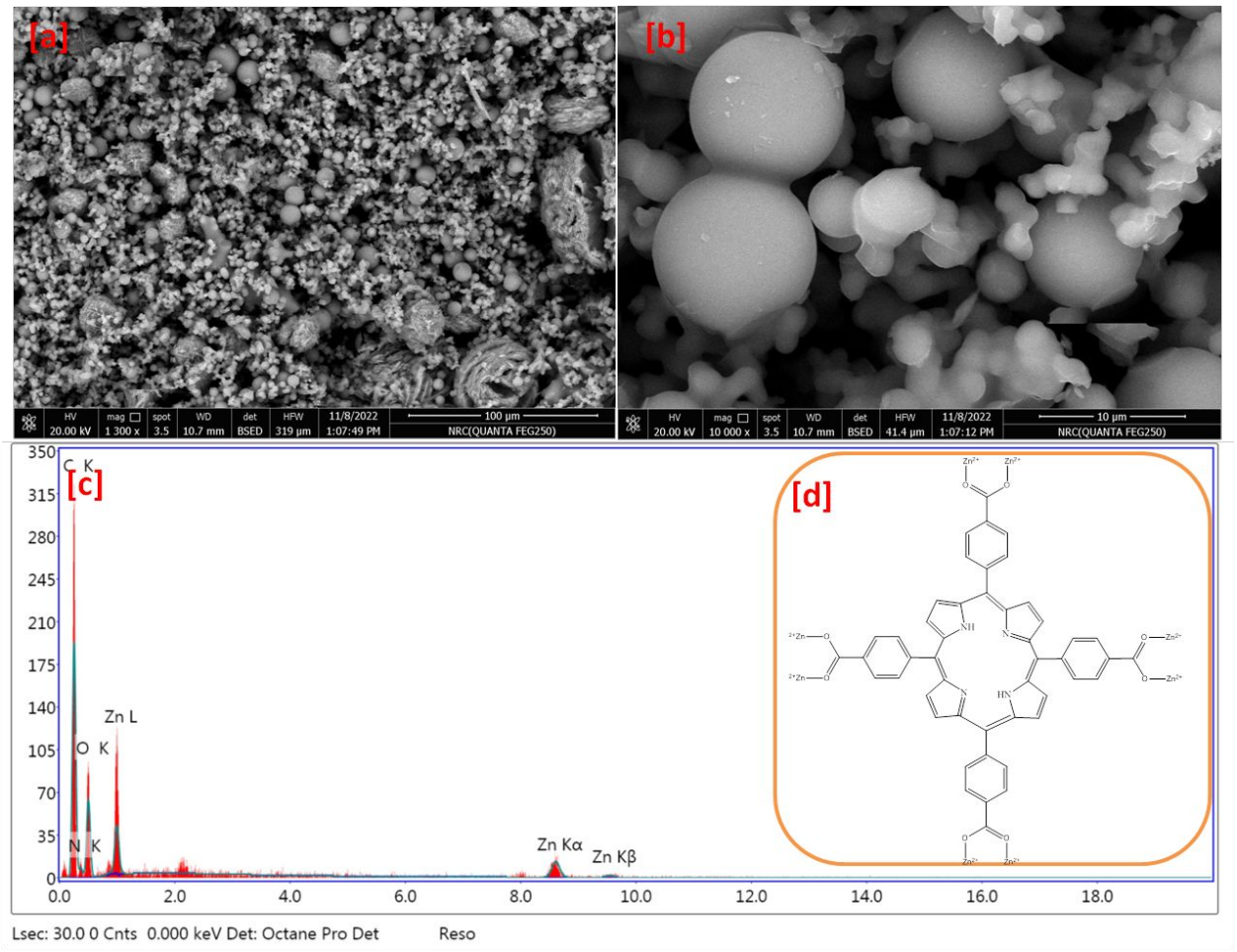

Figure 5. Micrographs and EDX analysis for the synthesized Zn-TCPP

SEM results of Fe-TCPP indicated that homogeneous nucleation with severely aggregated platelet-shaped crystals (Figure 6). EDX pattern of Fe-TCPP showed a clear appearance of carbon, oxygen and iron atoms in the chemical structure of prepared MOFs.

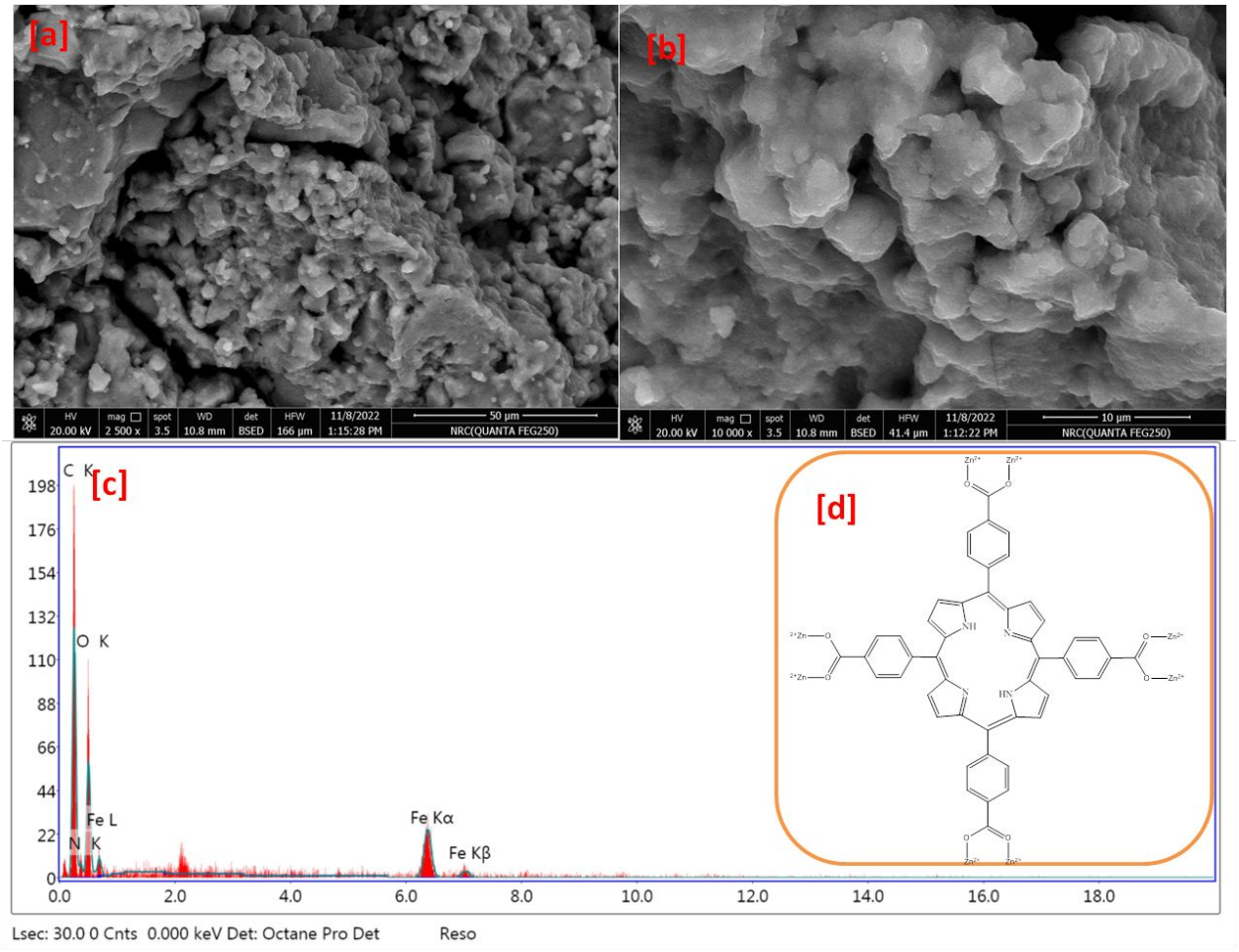

Figure 6. Micrographs and EDX analysis for the synthesized Fe-TCPP

3.2. Optimization of the adsorption process

The pH of the solution can significantly affect the surface charge of MOFs [42, 43], the methomyl adsorption rate was investigated under different pH ranging from 5 to 9. These ranges were chosen due to Cu-TCPP, Zn-TCPP, and Fe-TCPP can be dissolved in strongly alkaline media, figure 7a showed that the best adsorption rate was found at pH 7. The Langmuir (Figure 7b), and Freundlich isotherms (Figure 7c) were investigated to describe the behavior of Cu-TCPP, Zn-TCPP and Fe-TCPP in methomyl adsorption. Figure 7d showed that Fe-TCPP had a high adsorption capacity instead of Cu-TCPP and Zn-TCPP; this is because iron has a trivalent oxidation state that coordinates with more methomyl molecules. As is evident from the acquired data (R = 0.905 and 0.978), the Langmuir model fits the data. Additionally, the greatest methomyl pesticide adsorption capacities for Cu-TCPP, Zn-TCPP

and Fe-TCPP were 175, 190 and 270 mg g^{-1}, respectively (Table 1). The surface area of Cu-TCPP, Zn-TCPP and Fe-TCPP were 351.2, 374.5 and 418.3 mg g^{-1}, respectively.

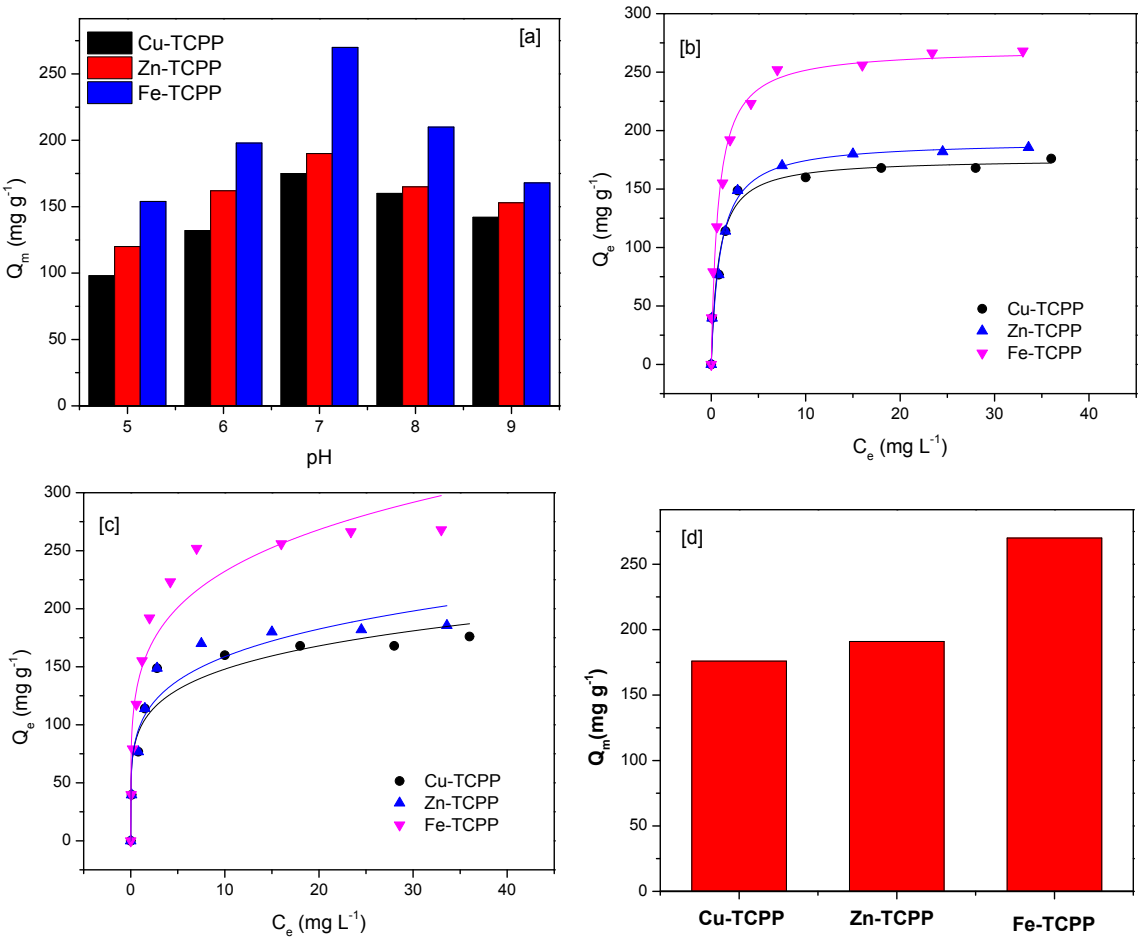

Figure 7. Effect of pH on the methomyl adsorption rate (initial concentration of methomyl was 100 mg L^{-1}, MOFs dose 300 mg L^{-1}, temperature 25 °C and time 180 minutes); isotherm profile of methomyl adsorption onto the synthesized porphyrin MOFs: [b] Langmuir model, [c] Freundlich model and [d] maximum adsorption capacity. (MOFs dose 300 mg L^{-1}, temperature 25 °C, time 180 minutes and pH was 7).

Table 1: Isotherm parameters of methomyl adsoprtion onto porphyrin MOFs.

Samples	BET surface area (m^2 g^{-1})	Freundlich				Langmuir			
		n	K_F	R^2	χ^2	Q_m (mg g^{-1})	K_L	R^2	χ^2
Cu-TCPP	351.2	5.45	97.016	0.919	332.46	175.94	1.290	0.975	99.80
Zn-TCPP	374.5	4.95	99.727	0.926	345.06	190.96	1.043	0.981	88.45
Fe-TCPP	418.3	4.81	143.986	0.928	664.01	270.07	1.360	0.984	145.25

Two pseudo-first order and pseudo-second order equations were studied to study the kinetics of methomyl adsorption on the surface of Cu-TCPP, Zn-TCPP and Fe-TCPP (Figure 8a,b). Figure 8a, b showed the adsorption kinetics for methomyl, the uptake processes quickly reached equilibrium. According to the data of R^2 (0.999) and low values of X^2, there is a stronger association between the kinetics of methomyl adsorption and the pseudo-second order than the pseudo-first order. This proves that van der Waals forces and the sharing of electrons between methomyl ions, Cu-TCPP, Zn-TCPP and Fe-TCPP were used to carry out the methomyl adsorption (Table 2). In addition, the best fit with the pseudo-second-order model indicates that the sorption process was focused on chemisorption [44, 45].

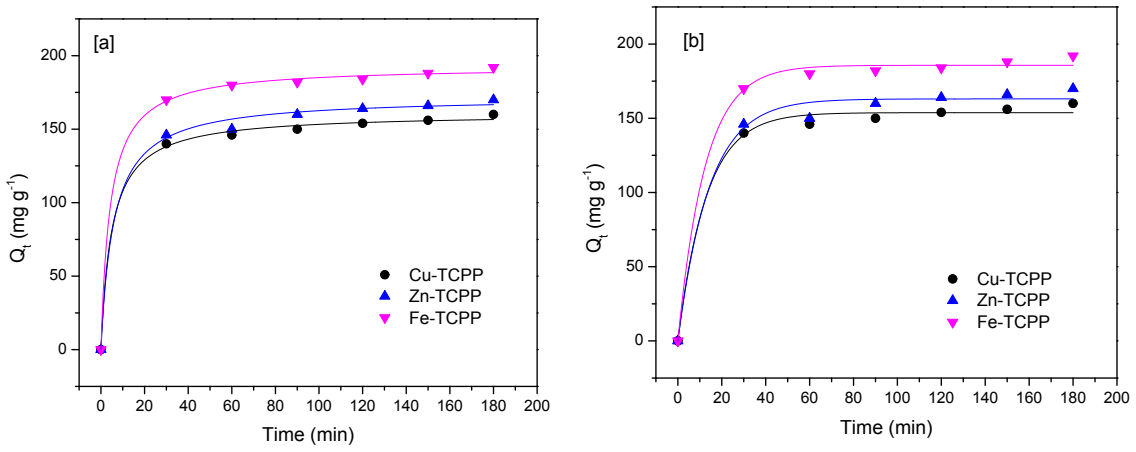

Figure 8. Kinetic of adsorption for methomyl onto the synthesized porphyrin MOFs; **[a]** pseudo-first order and **[b]** pseudo-second order. (Initial concentration of methomyl was 100 mg L^{-1}, MOFs dose was 300 mg L^{-1}, temperature 25 °C and pH was 7)

Table 2: Kinetic parameters of methomyl adsoprtion onto the porphyrin MOFs.

Samples	Q_e exp. (mg g^{-1})	pseudo-first-order				pseudo-second-order			
		Q_e (mg g^{-1})	K_1 (min^{-1})	R^2	χ^2	Q_e (mg g^{-1})	K_2 (L/mg.min)	R^2	χ^2
Cu-TCPP	160	153.78	0.07732	0.994	19.65	160.83	0.0012	0.998	5.75
Zn-TCPP	170	163.04	0.0704	0.989	37.30	172.04	0.003	0.996	12.86
Fe-TCPP	192	185.68	0.08065	0.996	15.82	192.89	0.0012	0.999	4.79

3.3. Possible Mechanism for methomyl adsorption with computational analysis (*Monte Carlo Simulation)*

The TCPP-MOFs possess two types of cavities/pores as illustrated in figure1. The large cavity (L) is located between the porphyrin linkers while the small cavity (S) is sandwiched between stacked porphyrin rings. MC simulation results revealed that the preferred adsorption sites for methomyl are in the (L) channel of the studied MOFs, as shown in Fig. 9. The Van der Waals is the main adsorption mechanism since the values for Van der Waals energies of a methomyl molecule in Fe TCPP, Zn TCPP, and CuTCPP were -27.65 kcal·mol^{-1}, -24.10 kcal·mol^{-1}, and -24.37 kcal·mol^{-1}; and the values for the electrostatic energies were -2.024 kcal·mol^{-1}, 7.97 kcal·mol^{-1}, and 9.59 kcal·mol^{-1}, respectively. The summation of both interaction types for the Fe TCPP, Zn TCPP, and Cu TCPP are -29.677, -16.133, and -14.78 kcal·mol^{-1}, respectively. This order is in agreement with the experimental Q_m values. Furthermore, the close contacts of methomyl with porphyrin MOFs were at a distance of (2.7~3.0) Å, as displayed in figure 9.

The average loading simulation at 101.33 kPa and 298 K of sorbed methomyl molecules per unit cell of Fe-TCPP, Zn-TCPP, and Cu-TCPP in the presence of water at 101.33 kPa and 298 K was 16.69, 13.36, and 9.69 molecules, while the average loading of water was 31.15, 35.62, and 101.2 molecules per unit cell, respectively. Thus, the average loading follows the order of Fe-TCPP > Zn-TCPP > Cu-TCPP, which again agrees with the Q_m order. Figure 10 displays the MC lowest-energy configurations of these systems which were followed by MD simulation.

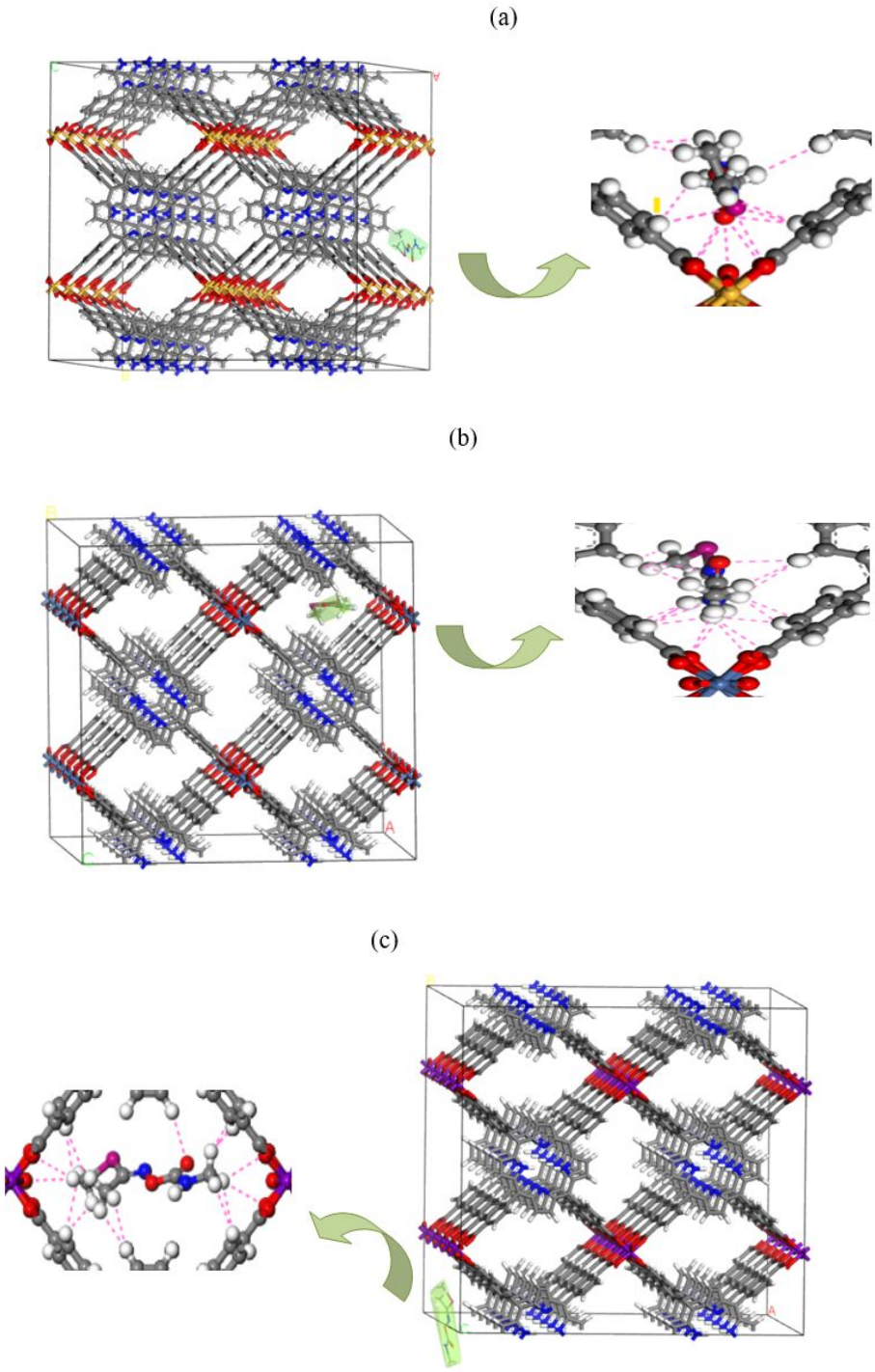

Figure 9. The lowest-energy structures for methomyl in Cu-TCCP (a), Fe-TCCP (b), and Zn-TCCP (c). Element colours: Cu (golden), Fe (stone), Zn (purple), C (gray), N (blue), H (white), O (red), and S (pink). For clarity purposes, the methomyl molecule is shaded lemon color**.**

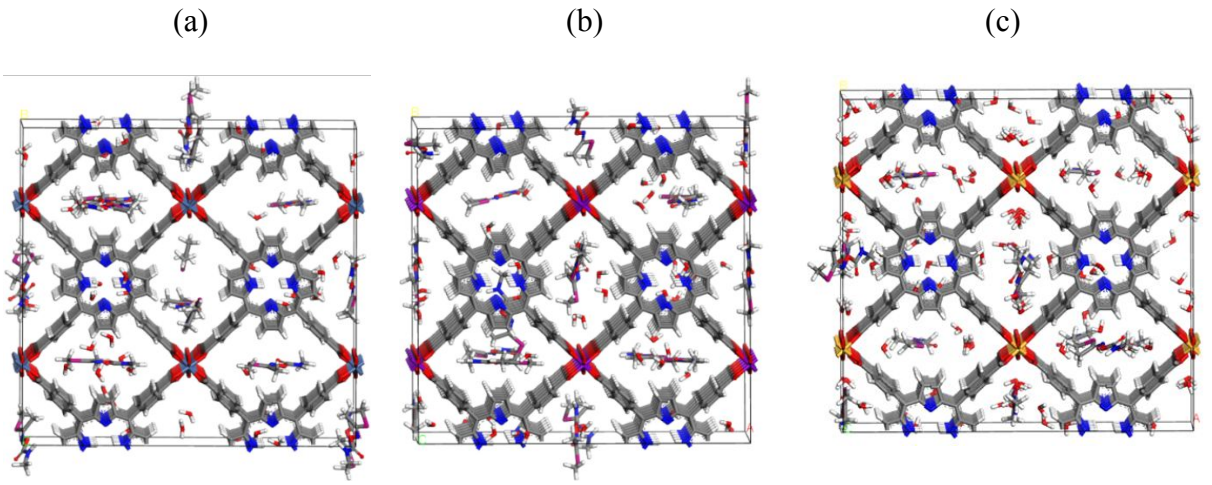

Figure 10. The lowest-energy configurations of the absorbed methomyl and water mixture in (a) Fe TCPP, (b) ZnTCPP, and (c) CuTCPP, as obtained by MC simulation at 101.33 kPa and 298 K.

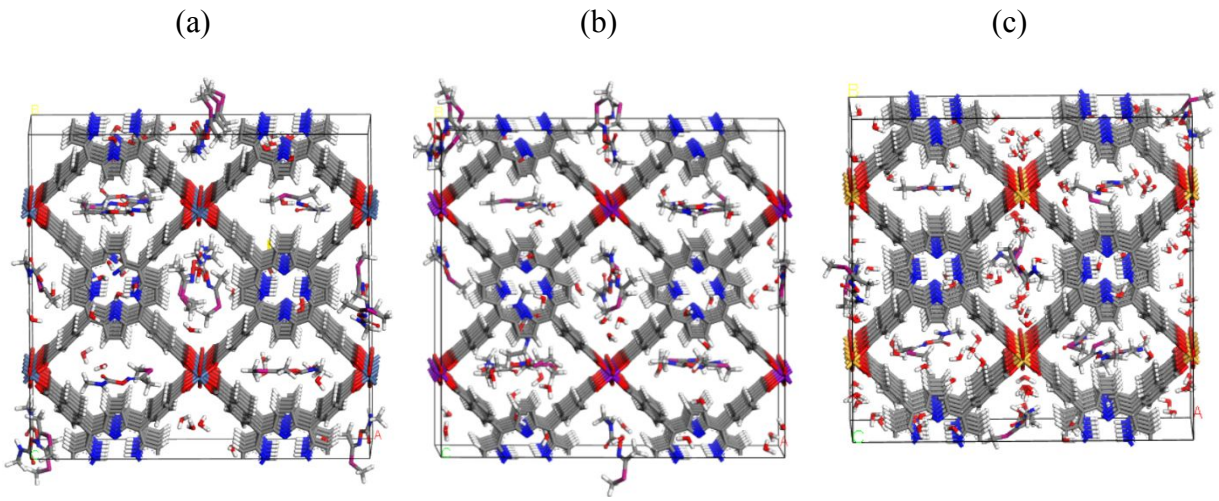

Figure 11. The final MD snapshots of (a) FeTCPP, (b) ZnTCPP, and (c) CuTCPP.

Molecular Dynamics Simulations

Figure 11 shows the final MD snapshots of the studied porphyrin-based MOFs. The interactions among methomyl, MOFs, and water molecules were quantified using the radial distribution function (RDF), which is computed from the simulation trajectories. RDF is a significant tool and defined as the probability of detecting any particle within the range of radial distances ($r + dr$) from a reference particle. Figure 12 (a, b) shows the intermolecular interaction of methomyl molecules with one another, where the hydrogen atom from the

amine group (H-N_{meth}) formed hydrogen bonds (H-bonds) with the oxygen atoms of the carbamate group (C=O_{meth} and C-O_{meth}). The H-bonds of (C=O_{meth}···H-N_{meth}) and (C-O_{meth}···H-N_{meth}) showed RDF peaks at 3.0 Å and 2.5 Å, respectively. Thus, the H-bonds strength of the latter interaction type is stronger than the former one. In the Cu-TCCP system, both interaction peaks are more intense than in the other MOFs. The hydrogen atom of the amine group (H-N_{meth}) also formed H-bonds with the oxygen atoms of the carboxylate groups of the porphyrin linkers (C=O_{MOF}) and oxygen of water molecules (OW). The (C=O_{MOF} ···H-N_{meth}) RDF shows a peak at 3.5 Å in the case of the Fe-TCCP and Zn-TCCP systems but not in the CuTCCP system (Figure 12c). The absence of this interaction in the Cu-TCCP system is probably because H-N grouped is already hydrogen bonded with carbamate's oxygen atoms (Figure 12a,b), as revealed from its high intensity compared with the other two MOFs. The H-N_{meth} formed weakly H-bonds with OW, as shown in figure 12d.

The H-bonds formation between the water hydrogen atoms (HW) and the polar atoms of methomyl molecule (i.e., O, N, and S) was analyzed and the corresponding RDFs are shown in figure 12(e,f). It is clear from figure 12e that the interaction between C-O_{meth} and HW is weaker than that between C=O_{meth} and HW. The interaction between HW and N=C_{meth} is weaker than the interaction between HW and S_{meth}. The intensity of the RDF peak corresponds to the interactions between HW and all polar atoms of methomyl molecule in Cu-TCPP is higher than that in Fe-TCPP and Zn-TCPP. The H-bonds formation between the HW and OW appeared at ~1.0 Å (Figure 12g), indicating water cluster formation.

A sharp peak appeared at ~2.5 Å between methyl groups of the methomyl molecules due to Van der Waals interactions (Figure 12h). The RDFs of the interactions between (C=O_{meth}) oxygen atoms and the metal atoms of all MOFs are shown in figure 12(i). The first RDFs peak of (C=O_{meth}····Fe_{MOF}), (C=O_{meth}····Zn_{MOF}), and (C=O_{meth}····Cu_{MOF}) appeared at a distance of ~4.5 Å, 4.5 Å, and 3.5 Å, respectively. This result concludes that the oxygen

atom of the $C=O_{meth}$ has a low affinity toward the metal atoms, and its interaction with Cu atoms is greater than that with Fe and Zn atoms. Figure 12(j) shows that the OW atoms have also a low affinity toward the Fe and Zn metals of the porphyrin-based MOFs, and showed more affinity toward Cu atoms.

The RDFs correspond to the interactions between polar atoms of methomyl and aromatic hydrogen (HA_{MOF}) atoms of benzene rings of the porphyrin-base MOFs are shown in Figure 12(k,l). The $HA_{MOF}\cdots(O\text{-}C_{meth}$, $O=C_{meth}$, S_{meth}, and $N=C_{meth})$ RDFs displayed peaks at a distance of ~(3.0, 2.7, 3.5, and 3.5) Å, respectively. The HA_{MOF} atoms have a higher affinity toward S_{meth} than $N=C_{meth}$, and also have a higher affinity toward $O\text{-}C_{meth}$ than $O=C_{meth}$. Figure 12(m) shows the RDF of the intermolecular interactions among the methomyl molecules which displayed a sharp peak at a distance of ~1.0 Å. This indicates that the methomyl molecules are aggregated inside the MOF cavities.

Table 3 showed that porphyrin based MOFs (Zn-TCPP, Cu-TCPP and Fe-TCPP) have high adsorption capacity rather than published materials. The obtained results showed that Zn-TCPP, Cu-TCPP and Fe-TCPP may be used as potential adsorbent for simultaneous removal of methomyl insecticide from wastewater.

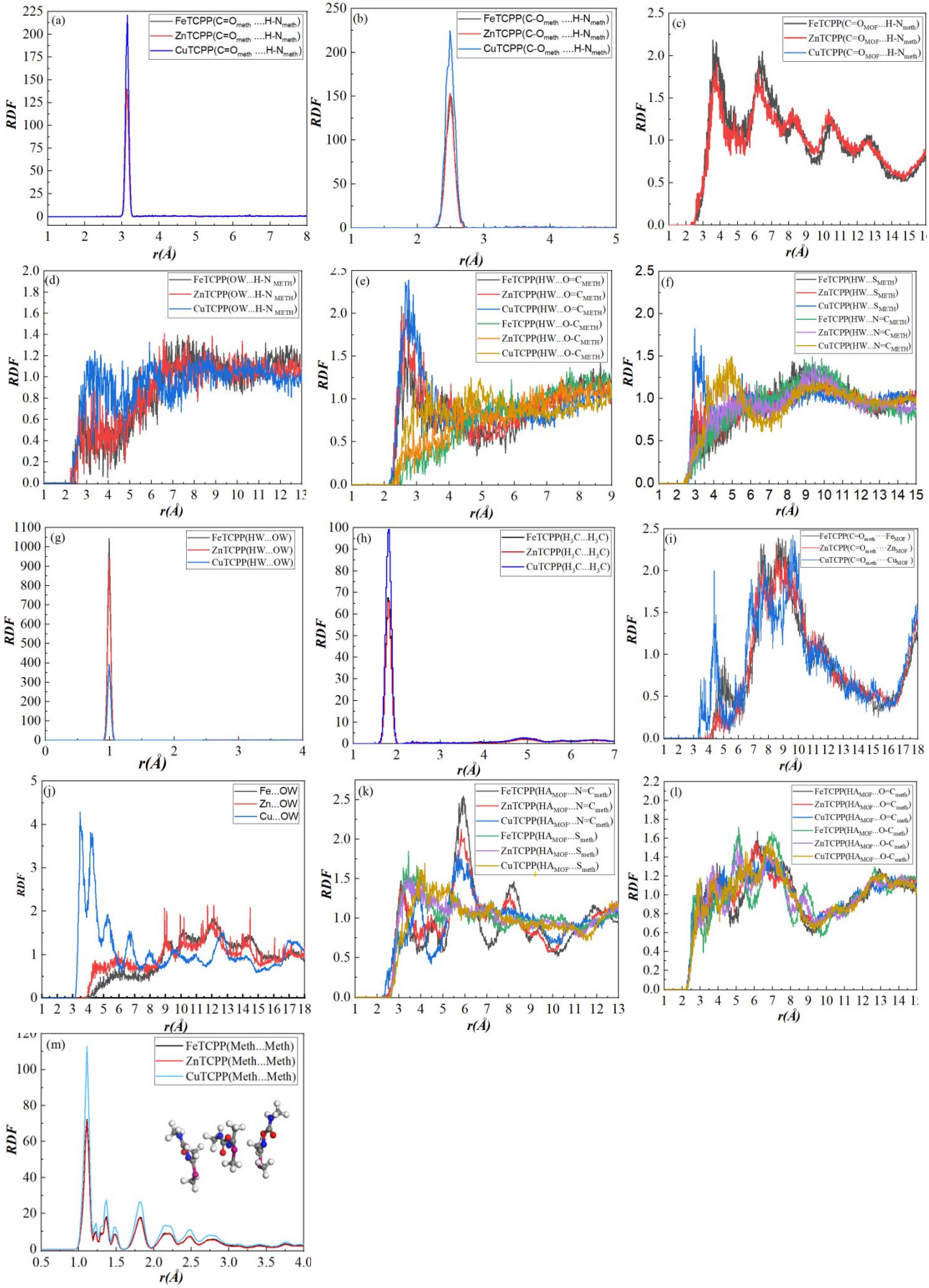

Figure 12. The RDFs analysis results from the MD simulation of methomyl and water in Fe-TCPP , Zn-TCPP, and Cu-TCPP.

Table 3: Comparison of adsorption capacities of methomyl on different adsorbs

Adsorption material	pH	Temperature ^0C	Surface area (m^2 g^{-1})	Maximum Adsorption capacity (mg g^{-1})	Reference
Cotton stack activated carbon (CTAC)	5.4	25	1600	72.85	[46]
Eucalyptus wood chips	7	25	4.02	32.42	[20]
Carbon xerogel	7	25	212.20	15.2	[47]
MN-100	7	25	815	21.6	[48]
60 % ZIF-8@Lignin	7	25		324.6	[28]
40%ZIF-8@Lignin	7	25		220.6	
20%ZIF-8@Lignin	7	25		324.6	
Co-Beta Zeolite particles	7.35	45	-	230.851	[49]
Ni-Al Hydrotalcite	4.5	25	-	43.02	[50]
Fe-TCPP	7	25	418.3	270.07	Current work
Zn - TCPP	7	25	374.5	190.95	
Cu- TCPP	7	25	351.2	175.93	

4. Conclusion

The current study investigated the adsorption properties of methomyl insecticide with three distinct porphyrin-MOFs (Zn-TCPP, Cu-TCPP, and Fe-TCPP). The elimination capacities of Zn-TCPP, Cu-TCPP, and Fe-TCPP are 175, 190, and 270 mg g^{-1}, respectively, from an initial concentration of 100 mg L^{-1} of methomyl insecticide. The results showed that Langmuir was more effective model to describe methomyl insecticide adsorbing than Freundlich, confirming that the adsorption process was spontaneous. In addition, the mechanisms of methomyl adsorption by Zn-TCPP, Cu-TCPP, and Fe-TCPP were determined using molecular dynamics simulations. Hydrogen bond formations, electrostatic interactions, pore filling are the possible mechanistic interactions between methomyl and porphyrin-MOFs. The results may provide new perspectives on the possibility of using Zn-TCPP, Cu-TCPP, and Fe-TCPP as adsorbents for pesticides from wastewater.

Author Contributions

Fatma Ayman.FM, Mohamed Taha, Ahmed A. Farghali, and Reda M. Abdelhameed are sharing in: Methodology, Data curation, Writing- Original draft preparation; Conceptualization, Supervision, Writing- Reviewing and Editing.

Acknowledgment

This publication is made possible by the generous support of the American people through the United States Agency for International Development (USAID). The contents are the responsibility of authors and do not necessarily reflect the views of USAID or the United States Government.

References

[1] F. Figueira, F.A.A. Paz, Porphyrin MOF-Derived Porous Carbons: Preparation and Applications, C, 7 (2021) 47.

[2] C. Wang, X. Liu, N.K. Demir, J.P. Chen, K. Li, Applications of water stable metal–organic frameworks, Chemical Society Reviews, 45 (2016) 5107-5134.

[3] S. Huh, S.-J. Kim, Y. Kim, Porphyrinic metal–organic frameworks from custom-designed porphyrins, CrystEngComm, 18 (2016) 345-368.

[4] D.D. La, H.P.N. Thi, Y.S. Kim, A. Rananaware, S.V. Bhosale, Facile fabrication of Cu (II)-porphyrin MOF thin films from tetrakis (4-carboxyphenyl) porphyrin and Cu (OH) 2 nanoneedle array, Applied Surface Science, 424 (2017) 145-150.

[5] R.M. Abdelhameed, M. Taha, H. Abdel-Gawad, B. Hegazi, Amino-functionalized Al-MIL-53 for dimethoate pesticide removal from wastewater and their intermolecular interactions, Journal of Molecular Liquids, 327 (2021) 114852.

[6] J. Lv, M. Wang, X. Chen, H. Qin, Y. Li, K. Yang, H. Zhang, Q. Zhang, P. Fu, Q. Fu, The Investigation of Hydrogen Adsorption in MOF NU-1501 with Different Metal Doping using Molecular Simulations, ChemistrySelect, 7 (2022) e202103725.

[7] R.M. Abdelhameed, M. El-Shahat, H. Abdel-Gawad, B. Hegazi, Efficient phenolic compounds adsorption by immobilization of copper-based metal-organic framework

anchored polyacrylonitrile/chitosan beads, International Journal of Biological Macromolecules, 240 (2023) 124498.

[8] R.M. Abdelhameed, O.M. Darwesh, M. El-Shahat, Titanium-based metal-organic framework capsulated with magnetic nanoparticles: Antimicrobial and photocatalytic degradation of pesticides, Microporous and Mesoporous Materials, 354 (2023) 112543.

[9] H.E. Emam, H.B. Ahmed, M. El-Shahat, H. Abdel-Gawad, R.M. Abdelhameed, Selective separation of chlorophyll-a using recyclable hybrids based on Zn-MOF@ cellulosic fibers, Scientific Reports, 13 (2023) 15208.

[10] M. El-Shahat, A.R. Wassel, R.M. Abdelhameed, Selective photo-oxidative coupling of amines to form C–N bonds using post synthetic modification of MIL-68-NH2 with metal acetylacetonate, New Journal of Chemistry, (2023).

[11] R.M. Abdelhameed, M. El-Shahat, Removable Visible-Light photocatalysts for Nitro-group reduction constructed from palladium decorated Ti-MOFs integrate onto fibers, Materials Science and Engineering: B, 290 (2023) 116309.

[12] A. Fateeva, J. Clarisse, G. Pilet, J.-M. Grenèche, F. Nouar, B.K. Abeykoon, F. Guegan, C. Goutaudier, D. Luneau, J.E. Warren, Iron and porphyrin metal–organic frameworks: insight into structural diversity, stability, and porosity, Crystal Growth & Design, 15 (2015) 1819-1826.

[13] J. Liu, Y. Yang, W. Zhu, X. Yi, Z. Dong, X. Xu, M. Chen, K. Yang, G. Lu, L. Jiang, Nanoscale metal− organic frameworks for combined photodynamic & radiation therapy in cancer treatment, Biomaterials, 97 (2016) 1-9.

[14] P. Ling, J. Lei, L. Zhang, H. Ju, Porphyrin-encapsulated metal–organic frameworks as mimetic catalysts for electrochemical DNA sensing via allosteric switch of hairpin DNA, Analytical chemistry, 87 (2015) 3957-3963.

[15] N. Sadeghi, S. Sharifnia, M.S. Arabi, A porphyrin-based metal organic framework for high rate photoreduction of CO2 to CH4 in gas phase, Journal of CO2 Utilization, 16 (2016) 450-457.

[16] C. Zhang, H. Li, C. Li, Z. Li, Fe-loaded MOF-545 (Fe): peroxidase-like activity for dye degradation dyes and high adsorption for the removal of dyes from wastewater, Molecules, 25 (2019) 168.

[17] Y. Kong, H. Lu, R. Wang, Q. Yang, B. Huang, Q. Zhou, W. Hu, J. Zou, Q. Chen, Adsorption characteristics of tetracycline hydrochloride and oxytetracycline by a MOF-525 (Co) metal organic framework, Colloids and Surfaces A: Physicochemical and Engineering Aspects, (2023) 132443.

[18] Y. Li, J. Pang, X.-H. Bu, Multi-functional metal–organic frameworks for detection and removal of water pollutions, Chemical Communications, 58 (2022) 7890-7908.

[19] T. Ahmad, M. Rafatullah, A. Ghazali, O. Sulaiman, R. Hashim, A. Ahmad, Removal of pesticides from water and wastewater by different adsorbents: a review, Journal of Environmental Science and Health, Part C, 28 (2010) 231-271.

[20] A. Srikhaow, W. Chaengsawang, T. Kiatsiriroat, P. Kajitvichyanukul, S.M. Smith, Adsorption kinetics of imidacloprid, acetamiprid and methomyl pesticides in aqueous solution onto eucalyptus woodchip derived biochar, Minerals, 12 (2022) 528.

[21] J. Zolgharnein, A. Shahmoradi, J. Ghasemi, Pesticides removal using conventional and low-cost adsorbents: a review, Clean–Soil, Air, Water, 39 (2011) 1105-1119.

[22] M. Tamimi, S. Qourzal, N. Barka, A. Assabbane, Y. Ait-Ichou, Methomyl degradation in aqueous solutions by Fenton's reagent and the photo-Fenton system, Separation and Purification Technology, 61 (2008) 103-108.

[23] Z. Lin, W. Zhang, S. Pang, Y. Huang, S. Mishra, P. Bhatt, S. Chen, Current approaches to and future perspectives on methomyl degradation in contaminated soil/water environments, Molecules, 25 (2020) 738.

[24] M. Qiu, L. Liu, Q. Ling, Y. Cai, S. Yu, S. Wang, D. Fu, B. Hu, X. Wang, Biochar for the removal of contaminants from soil and water: a review, Biochar, 4 (2022) 19.

[25] Q. Li, Z. Chen, H. Wang, H. Yang, T. Wen, S. Wang, B. Hu, X. Wang, Removal of organic compounds by nanoscale zero-valent iron and its composites, Science of the Total Environment, 792 (2021) 148546.

[26] S. Yu, H. Pang, S. Huang, H. Tang, S. Wang, M. Qiu, Z. Chen, H. Yang, G. Song, D. Fu, Recent advances in metal-organic framework membranes for water treatment: A review, Science of the Total Environment, 800 (2021) 149662.

[27] M. Qiu, B. Hu, Z. Chen, H. Yang, L. Zhuang, X. Wang, Challenges of organic pollutant photocatalysis by biochar-based catalysts, Biochar, 3 (2021) 117-123.

[28] R. Abdelhameed, M. Hasanin, H. Abdel-Gawad, B. Hegazi, Engineering ZIF-8 morphology for uptake of methomyl residues from wastewater by combining it with extracted lignin as an antibacterial, (2022).

[29] Q. Yang, J. Wang, W. Zhang, F. Liu, X. Yue, Y. Liu, M. Yang, Z. Li, J. Wang, Interface engineering of metal organic framework on graphene oxide with enhanced adsorption capacity for organophosphorus pesticide, Chemical Engineering Journal, 313 (2017) 19-26.

[30] R.M. Abdelhameed, M. Taha, H. Abdel-Gawad, F. Mahdy, B. Hegazi, Zeolitic imidazolate frameworks: Experimental and molecular simulation studies for efficient capture of pesticides from wastewater, Journal of Environmental Chemical Engineering, 7 (2019) 103499.

[31] R.M. Abdelhameed, H. Abdel-Gawad, M. Elshahat, H.E. Emam, Cu–BTC@ cotton composite: design and removal of ethion insecticide from water, Rsc Advances, 6 (2016) 42324-42333.

[32] R.M. Abdelhameed, H.E. Emam, Modulation of metal organic framework hybrid cotton for efficient sweeping of dyes and pesticides from wastewater, Sustainable Materials and Technologies, 31 (2022) e00366.

[33] A. Harada, H. Yamaguchi, K. Okamoto, H. Fukushima, K. Shiotsuki, M. Kamachi, Control of photoinduced electron transfer from zinc-porphyrin to methyl viologen by supramolecular formation between monoclonal antibody and zinc-porphyrin, Photochemistry and photobiology, 70 (1999) 298-302.

[34] E.-Y. Jeong, M.B. Ansari, Y.-H. Mo, S.-E. Park, Removal of Cu (II) from water by tetrakis (4-carboxyphenyl) porphyrin-functionalized mesoporous silica, Journal of hazardous materials, 185 (2011) 1311-1317.

[35] G. Garcia, V. Sol, F. Lamarche, R. Granet, M. Guilloton, Y. Champavier, P. Krausz, Synthesis and photocytotoxic activity of new chlorin–polyamine conjugates, Bioorganic & medicinal chemistry letters, 16 (2006) 3188-3192.

[36] Z.A. Alothman, A.H. Bahkali, M.A. Khiyami, S.M. Alfadul, S.M. Wabaidur, M. Alam, B.Z. Alfarhan, Low cost biosorbents from fungi for heavy metals removal from wastewater, Separation Science and Technology, 55 (2020) 1766-1775.

[37] A.A. Alqadami, S.M. Wabaidur, B.-H. Jeon, M.A. Khan, Co-hydrothermal valorization of food waste: process optimization, characterization, and water decolorization application, Biomass Conversion and Biorefinery, (2023) 1-12.

[38] T. Rhauderwiek, S. Waitschat, S. Wuttke, H. Reinsch, T. Bein, N. Stock, Nanoscale synthesis of two Porphyrin-based MOFs with gallium and indium, Inorganic Chemistry, 55 (2016) 5312-5319.

[39] R.L. Akkermans, N.A. Spenley, S.H. Robertson, Monte Carlo methods in materials studio, Molecular Simulation, 39 (2013) 1153-1164.

[40] M.A. Addicoat, N. Vankova, I.F. Akter, T. Heine, Extension of the universal force field to metal–organic frameworks, Journal of chemical theory and computation, 10 (2014) 880-891.

[41] A.K. Rappe, W.A. Goddard III, Charge equilibration for molecular dynamics simulations, The Journal of Physical Chemistry, 95 (1991) 3358-3363.

[42] R. Abdelhameed, H. Abdel-Gawad, C. Silva, J. Rocha, B. Hegazi, A. Silva, Kinetic and equilibrium studies on the removal of 14 C-ethion residues from wastewater by copper-based metal–organic framework, International Journal of Environmental Science and Technology, (2018) 1-12.

[43] R.M. Abdelhameed, R.A. Ismail, M. El-Naggar, E.S. Zarie, R. Abdelaziz, M.T. El Sayed, Post-synthetic modification of MIL-125 with bis-quinoline Mannich bases for removal of heavy metals from wastewater, Microporous and Mesoporous Materials, 279 (2019) 26-36.

[44] Y.-S. Ho, G. McKay, Pseudo-second order model for sorption processes, Process biochemistry, 34 (1999) 451-465.

[45] S. Wang, H. Li, Kinetic modelling and mechanism of dye adsorption on unburned carbon, Dyes and pigments, 72 (2007) 308-314.

[46] M. El-Geundi, M. Nassar, T. Farrag, M. Ahmed, Methomyl adsorption onto Cotton Stalks Activated Carbon (CSAC): equilibrium and process design, Procedia Environmental Sciences, 17 (2013) 630-639.

[47] N.A. Fathy, A.A. Attia, B. Hegazi, Nanostructured activated carbon xerogels for removal of methomyl pesticide, Desalination and water treatment, 57 (2016) 9957-9970.

[48] C.-F. Chang, C.-Y. Chang, K.-E. Hsu, P. Chiang, Removal of methomyl pesticide by adsorption using novel hypercrosslinked polymer of macronet MN-100, Journal of the Chinese Institute of Environmental Engineering, 17 (2008) 311-318.

[49] P. Stojisavljević, N. Vulović, Z. Veličković, D. Mijin, S. Stupar, D. Dinić, N. Ivanković, Investigation on the adsorption of the carbamate pesticide methomyl from aqueous solution using modified co-beta zeolite particles, Science of Sintering, (2023) 4-4.

[50] R.M. Jamhour, Determination of Methomyl and Imidacloprid in Water by Adsorption on Ni-Al HydrotalciteUsing HPLC, Canadian Chemical Transactions, 2 (2014) 535-545.